Journal of Applied Mechanics and Technical Physics, Vol. 37, No. 6, 1996

EFFECT OF A PYCNOCLINE ON FORCES EXERTED BY INTERNAL WAVES ON A STATIONARY CYLINDER

N. V. Gavrilov and E. V. Ermanyuk

UDC 532.59

Full-scale [1] and laboratory [2, 3] experiments show that internal waves can have a significant dynamic effect on underwater apparatus and marine structures. In the case of a sudden jump in density at the interface, the methods developed for surface waves are applicable to studies of forces acting on bodies in a fluid layer with a constant density. The problem of the rolling of a body located above (beneath) a pycnocline has been solved theoretically [4, 5]. If the dimensions of the body are small compared with the wavelength, the problem can be simplified [6]. A semi-empirical model of the force action of internal waves was proposed in [7].

Under the action of internal waves on bodies located in a zone with a varying density, a number of interesting dynamic effects occur. The possibility of mutual compensation of the hydrostatic and inertial components of wave loading was proved experimentally in [2] for three-dimensional bodies. The nonlinear effect of frequency doubling of the horizontal force for bodies located at the interface is shown in [3]. It should be noted that the presence of a layer with a continuously varying density results in the occurrence of complex diffraction effects due to energy redistribution among the different modes of wave motions of the fluid [8, 9].

This paper reports the results of measurements of the forces exerted by internal waves on an elliptic cylinder under stratification conditions with a large density-gradient layer (pycnocline). The wave loads are shown to be significantly dependent on the pycnocline thickness. It is found that for a body immersed in a zone with a continuously varying density, there is a direction along which the force action of waves is maximal, and the force action perpendicular to this direction is smaller by a factor of 5–6. The effect is associated with the occurrence of additional diffraction loads.

The experiments were performed in a hydrodynamic test tank (Fig. 1) 450 cm long, 20 cm wide, and 60 cm high, in which nearly two-layer stratification was created. The upper layer consisted of distilled water with density $\rho_1 = 0.999$ g/cm^3, and the lower layer consisted of an aqueous solution of glycerin with density $\rho_2 = 1.011$ g/cm^3. The waves in the pycnocline were generated by a half-cylinder 1, which accomplished harmonic oscillations along the end wall of the test tank. The opposite end of the test tank was equipped with a wave breaker 2 in the form of an inclined plate. The forces acting on an elliptic cylinder 3 with a length of 19.8 cm were studied. The small axis of the cylinder was $b = 3$ cm, and the ratio of the axes was 2:1. The clearances between the ends of the cylinder and the side walls of the test tank did not exceed 0.1 cm.

The measurements were performed by two-component balances 4 [3], whose minimum natural frequency with the cylinder suspended on them in water was 2.4 Hz. The maximum force frequency in the experiments did not exceed 0.21 Hz, and, therefore, the natural oscillations of the system did not influence the measured forces. A system of strings 5 and streamlined arms 6 transferred the forces to elastic elements 7. The deformations of the elastic elements were measured by induction displacement sensors. The maximum amplitude of wave loading was $1.1 \cdot 10^{-3}$ N. The elastic displacement of the elliptic cylinder under the action of this force did not exceed $5 \cdot 10^{-3}$ mm. Special experiments showed that in wave-load measurements the error due to the presence of submerged elements of the balances was not more than 0.5%.

Lavrent'ev Institute of Hydrodynamics, Russian Academy of Sciences, Novosibirsk 630090. Translated from Prikladnaya Mekhanika i Tekhnicheskaya Fizika, Vol. 37, No. 6, pp. 61–69, November–December, 1996. Original article submitted July 12, 1995; revision submitted August 22, 1995.

0021-8944/96/3706-0825 $15.00

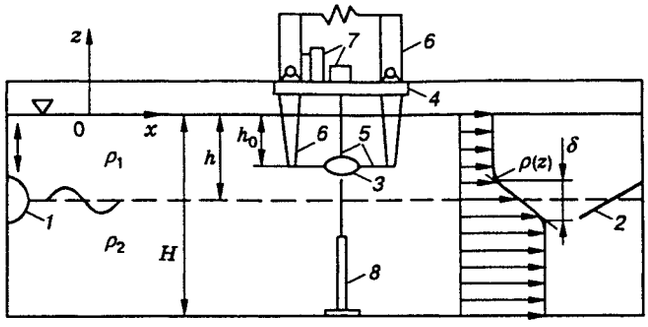

Fig. 1

The internal-wave parameters were recorded by resistive-type wavemeters 8 of the type of [10]. The signals from the wavemeters and force sensors were processed on a computer. The density distribution along the vertical was measured by sensors with horizontally located electrodes, whose principle of operation is based on the fact that a mixture of water with glycerin is a conductor. With a small difference between the densities (as, e.g., in these experiments), the conductivity of the mixture is directly proportional to the glycerin concentration (i.e., to the density). Hence, the density profile can be readily obtained from the voltage measured by the sensor at various points along the vertical if the densities ρ_1 and ρ_2 near the free surface and at the bottom are known. The densities were measured by standard areometers. The depth distribution of the density was measured prior to and after the experiments. Because of the smallness of the coefficient of glycerin diffusion in water, the distribution parameters were practically constant during one series of experiments. In the free-surface coordinate system (the z axis is directed upward, and the x axis is directed along the wave propagation), the density distribution established with time is close to the relation

$$\rho(z) = \rho_0 - \frac{\varepsilon\rho_1}{2}\tanh\frac{2(z+h)}{\delta}, \quad \rho_0 = \frac{\rho_2+\rho_1}{2}, \quad \varepsilon = \frac{\rho_2-\rho_1}{\rho_1}, \tag{1}$$

where $h = 14$ cm is the depth of the upper fluid layer, and δ is a parameter that characterizes the pycnocline thickness. The total fluid depth in the test tank was $H = 45$ cm.

The wavemaker generates, strictly speaking, all modes of wave motion of the fluid. However, if the oscillations of the wavemaker have a small amplitude and the diameter of the oscillating half-cylinder is large compared with the pycnocline thickness, the higher modes are weakly generated and decay rapidly with distance from the perturbation source. The measurement zone was separated from the wavemaker by 180 cm. Observation of the wave motion showed that the perturbation was determined by the first mode. As is known, the first mode of wave motion of a two-layer fluid having a zone with a continuously varying density satisfies the dispersion relation [8]

$$\omega^2 = \varepsilon gk/(k\gamma + \operatorname{cotanh} kh + \operatorname{cotanh} k(H-h)), \tag{2}$$

where k is the wavenumber, ω is the wave frequency, and γ is the typical width of the smeared zone. Measurements show that relation (2) approximates well the experimental results, provided that $\gamma = \delta$.

The amplitude of first-mode oscillations was determined with correction for the data of the dynamic calibration of the wavemeters. For this, the vertical harmonic oscillations relative to the unperturbed interface were imparted to the wavemeters, and this modeled operation under perturbation conditions. The calibration results are shown in Fig. 2 as the curve of the dimensionless amplitude of the output signal and $\bar{A} = A/A_0$ versus the frequency ω for various $\bar{\delta}$, where A is the dynamic amplitude of the output signal, and A_0 is a static amplitude that corresponds to the difference between the output signals measured for the extreme upper and lower positions of the wavemeters after the attenuation of the transient process. The value of $\bar{\delta}$ was determined from the measured density profile. The phase shift between the oscillations of the wavemeter and the output signal was practically absent. Such a strong dependence of the curves on $\bar{\delta}$ is indicative of the importance of dynamic calibration of wavemeters in measurements of internal-wave amplitudes using resistive sensors under

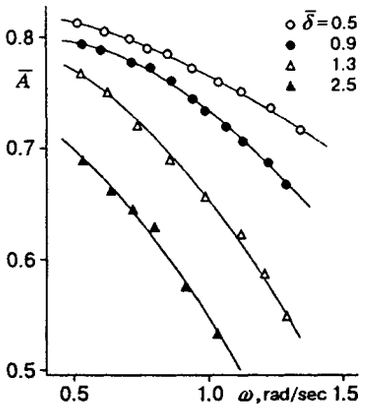

Fig. 2

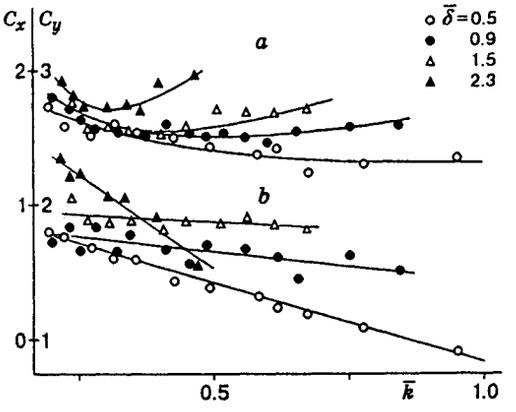

Fig. 3

conditions of a continuously varying density as a function of depth.

In the system described, the force action of the first internal-wave modes on the horizontal stationary elliptic cylinder is determined by the following dimensionless parameters:

$$h/b, \quad H/b, \quad \zeta = h_0/b, \quad \eta = a/b, \quad \bar{\delta} = \delta/b, \quad \bar{k} = kb, \quad \beta = b\sqrt{\omega/\nu}.$$

Here a is the amplitude of internal waves (the vertical displacement of the fluid particles averaged over the pycnocline thickness; the error of measurements of a using wavemeters of the type of [10] did not exceed 7%), h_0 is the distance from the free surface to the center of the cylinder, and ν is the kinematic fluid viscosity. The values of the parameters h/b and H/b were fixed.

Three variants of location of the body relative to the pycnocline were studied: in the middle of the upper layer for $\zeta = 2.0$ and near the interface in the upper and lower layer for $\zeta = 3.5$ and $\zeta = 5.4$, respectively.

For each submersion, the parameter characterizing the pycnocline thickness varied within $0.45 < \bar{\delta} < 2.5$. The pycnocline thickness varied due to glycerin diffusion. The value $\bar{\delta} = 0.9$ was reached 24 h after filling of the upper liquid layer [10]. For each pair of values of ζ and $\bar{\delta}$, the wave loads were measured as functions of incident-wave amplitude and length. The corresponding typical parameters were varied within $0.1 < \eta < 0.4$ and $0.2 < \bar{k} < 1.1$.

It turned out that for small values of η the wave loads are proportional to the wave amplitude within the measurement error in all series of experiments. It is known that if the amplitudes of particle motions are small compared with the dimensions of the body, the effect of the fluid viscosity is insignificant, and a change in the Stokes parameter β has practically no effect on wave loads [11, 12]. A similar result was also obtained in the present work. The Stokes parameter was varied within $20 < \beta < 30$. Note that the kinematic viscosity of the upper and lower fluid layers differed by not more than 10%.

The amplitudes of wave loads were normalized to the scale of the inertial forces $\rho_0 S\dot{u}_x$ and $\rho_0 S\dot{u}_y$ so that

$$C_x = F_x/\rho_0 S\dot{u}_x, \quad C_y = F_y/\rho_0 S\dot{u}_y, \tag{3}$$

where $\dot{u}_x$ and $\dot{u}_y$ are the amplitudes of the local accelerations of fluid particles at a depth corresponding to the center of the pycnocline; S is the cross-sectional area of the elliptic cylinder; F_x and F_y are the amplitudes of the horizontal and vertical forces acting on the cylinder with a unit length.

Use of the first-order theory [8] taking into account the dispersion relation (2) gives the following estimated amplitudes of the local accelerations:

$$\begin{aligned} \dot{u}_x &= \frac{a\omega^2 \cosh kh_0}{\sinh kh}, \quad \dot{u}_y = \frac{a\omega^2 \sinh kh_0}{\sinh kh} && \text{for} \quad -h < z < 0, \\ \dot{u}_x &= \frac{a\omega^2 \cosh k(H-h_0)}{\sinh k(H-h)}, \quad \dot{u}_y = \frac{a\omega^2 \sinh k(H-h_0)}{\sinh k(H-h)} && \text{for} \quad -H < z < -h. \end{aligned} \tag{4}$$

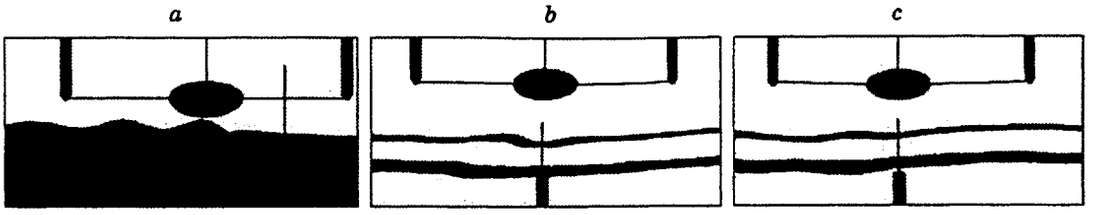

Fig. 4

This normalization makes it possible to represent most simply the experimental data for a body located in a homogeneous fluid layer (see, e.g., [11, 13]). For a body located in the zone with a continuously varying density, the total force action is determined not only by inertial loads, but by the diffraction effects and the effect of the varying buoyancy. In this case, however, to divide the total experimentally measured force into components of various physical natures, one should employ additional hypotheses. Therefore, this work uses calibration (3) for all cases of body submersion. It should be noted that use of relations (4) for fluid particles located within the pycnocline gives overstated estimates which should be regarded, in this case, simply as normalization parameters.

The results of measurements of forces acting on the elliptic cylinder located in the upper fluid layer for $\zeta = 2$ are given as curves of C_x and C_y versus the dimensionless wave number $\bar{k}$ for various $\bar{\delta}$, respectively, in Fig. 3a and 3b, For all values of $\bar{\delta}$, the buoyancy has practically no influence. The results, however, show that even in this case, the force coefficients are significantly dependent on pycnocline thickness.

In the case of a sudden density jump ($\bar{\delta} = 0.5$) the total force coefficient is $C_x \sim 1.5$ over a wide range of $\bar{k}$, i.e., it is close to the theoretical coefficient of the inertial force for an elliptic cylinder with a ratio of the axes of 2:1 immersed in the flow of an infinite ideal fluid that executes translational oscillations along the large axis of the ellipse (for oscillations along the small axis of the ellipse, the corresponding coefficient is 3 [14]). The increase in C_x with an increase in increasing $\bar{\delta}$ is obviously due to the relative decrease in the thickness of the upper fluid layer with constant density and to the effect of flow contraction.

The curve of C_y versus $\bar{\delta}$ is more complicated and nonmonotonic over some range of dimensionless wavenumbers $\bar{k}$. Attention is drawn to the linear curve $C_y = 2 - 1.2\bar{k}$ in the case of a sudden density jump ($\bar{\delta} = 0.5$). It should be noted that for all combinations of $\bar{\delta}$ and $\bar{k}$ the values of C_y are considerably smaller than 3.

The phase shifts between pycnocline oscillations and the loads acting on the elliptic cylinder was $104.9° \pm 1.5°$ and $201.2° \pm 2.2°$ for the horizontal and vertical forces, respectively. The effect of the parameter $\bar{\delta}$ on the phase shifts in this series of experiments was not observed. When the elliptic cylinder is located near the pycnocline, the phase shifts were not measured, and the parameters of incident internal waves were recorded at a point 12 cm from the center of the cylinder.

It can be assumed that the character of the curves of C_x and C_y versus $\bar{k}$ and $\bar{\delta}$ is due to the generation of the higher wave modes of fluid motion. The typical pattern of wave diffraction on the pycnocline in the case of a thin pycnocline ($\bar{\delta} = 0.5$) is given in Fig. 4a (the waves propagate from right to left). In the parameter range considered, the incident wave was represented by the first mode, and the effects of wave reflection were practically absent. The frequency of the incident wave was $\omega = 0.745$ rad/sec, and the wavelength was $\lambda = 56$ cm. Second-order waves are observed behind the body. These waves have a double oscillation frequency in comparison with the frequency of the incident waves. The main difference from similar effects observed for surface waves (see, e.g., [13, 15]) is that, by virtue of the dispersion relation (1), even for small $\bar{\delta}$ the second-order waves λ' have a very small length (in the above example, it is $\lambda' = 7.5$ cm) and do not influence the forces acting on the body. Spectral analysis of the record of the force sensor performed on a computer showed that the amplitude of the second harmonics is negligible compared with the amplitude of the first harmonics (less than 2%).

In addition, if the frequency of the incident waves $\omega > N_{\max}/2$ (where $N_{\max}$ is the maximum Brunt-

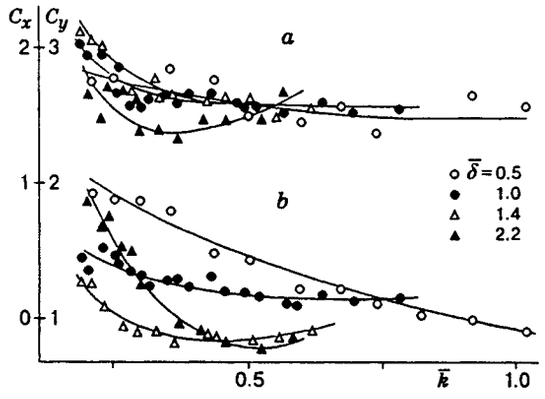

Fig. 5

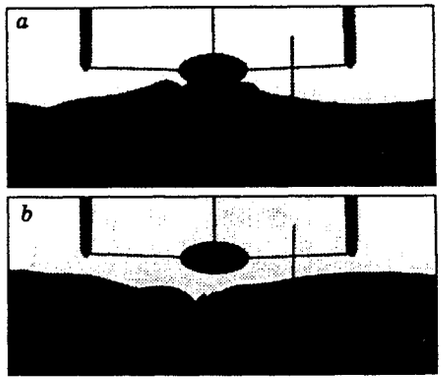

Fig. 6

Väisälä frequency $N(z) = \sqrt{-g\partial\rho/\rho\partial z}$), second-order progressive waves are not generated. This effect is illustrated in Fig. 4b and 4c (the interlayer boundaries are darkened) for $\bar{\delta} = 1.5$ and $N_{\max} = 1.58$ rad/sec. For this value of $\bar{\delta}$, second-mode wave oscillations can be generated. If $\omega < 0.5N_{\max}$, the wave pattern behind the body is the sum of the first- and second-mode oscillations, and also of second-order waves (Fig. 4b, $\omega = 0.773$ rad/sec, $\lambda = 44$ cm, and $\lambda' = 6.5$ cm). For $\omega > 0.5N_{\max}$, only first- and second-mode waves are observed behind the body (Fig. 4c, $\omega = 0.83$ rad/sec, $\lambda = 37$ cm, and $\lambda_2 = 11.5$ cm is the length of the second mode). It should be noted that oscillations with a frequency of $0.5N_{\max}$ correspond to the wavelength $\lambda = 42$ cm.

In practice, because of the viscous dissipation of internal waves, the upper threshold of frequencies of the incident waves is limited $\omega \sim 0.7N_{\max}$. This is responsible for narrowing of the studied range of $\bar{k}$ with an increase in $\bar{\delta}$.

As the elliptical cylinder approaches the interface, the effect of the parameter $\bar{\delta}$ increases. The curves of C_x and C_y versus $\bar{k}$ and $\bar{\delta}$ for $\zeta = 3.5$ (the body is in the upper layer near the interface) are shown, respectively, in Figs. 5a and 5b.

For small values of $\bar{\delta}$, the effect of the varying buoyancy force was negligibly small, which allows one to compare the results of this series of experiments with the previous results obtained under similar conditions. Comparison of Figs. 3 and 5 shows that for $\zeta = 3.5$ the values of C_x and C_y somewhat increase for long waves ($\bar{k} < 0.5$), and the linear curve of C_y versus $\bar{k}$ is somewhat deviated.

The curve of C_x versus $\bar{\delta}$ becomes nonmonotonic. With an increase in $\bar{\delta}$, the body is partially immersed in the pycnocline, and the amplitudes of the horizontal force increase under the action of incident long waves. This appears to be due to the occurrence of additional loads from wave impact on the body. The observed flow pattern of the type of slamming is shown in Fig. 6 (the waves propagate from right to left). For a more clear illustration, waves of large amplitude are shown. Upon wave impact, jet fluid flow forms, but, because of the small difference between the densities, the perturbation propagates almost horizontally. Near the end edge of the cylinder, a vortex forms which then separates and moves downward together with the wave (Fig. 6b). From the left of the cylinder, second-order perturbations are clearly seen. With a further increase in pycnocline thickness, the cylinder turns out to be completely submerged in the zone with a continuously varying density, and the coefficient of the horizontal force C_x again decreases.

The vertical wave loads decrease with an increase in $\bar{\delta}$. This is due to the fact that the inertial forces and the buoyancy forces act in counterphase, and their mutual compensation is possible [7]. Introducing the hypothesis that the density distribution does not change with internal-wave passage and can be considered linear near the body, one can easily show that the ratio of the inertial forces and buoyancy forces is determined by the parameter $\alpha = \omega^2/N^2(z_0)$, which has the physical meaning of Froude's number. For $\alpha < 1$, buoyancy forces dominate, and for $\alpha > 1$, inertial forces (for a homogeneous fluid, $\alpha \to \infty$). An increase in C_y with

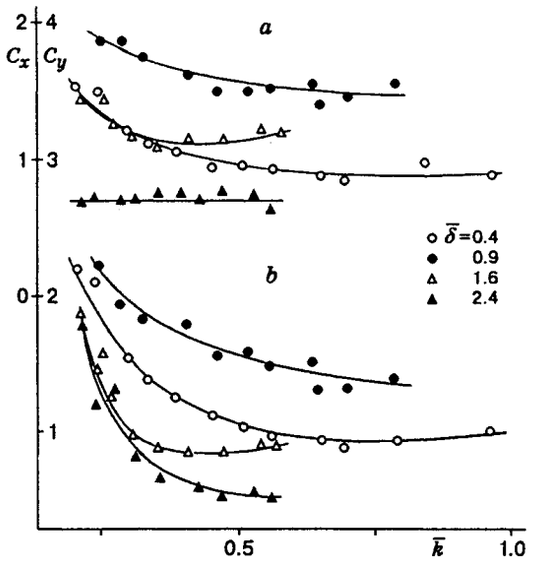

Fig. 7

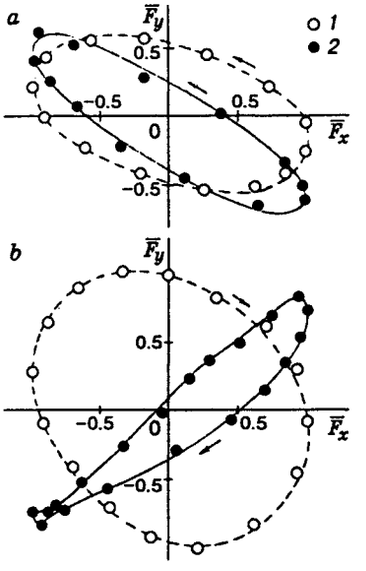

Fig. 8

increasing pycnocline thickness for small values of $\bar{k}$ is a peculiarity of the chosen normalization (3) and (4), since for long waves the relative role of buoyancy forces increases.

The curves of C_x and C_y for the body located beneath the pycnocline ($\zeta = 5.4$) are given in Figs. 7a and 7b. A distinguishing feature of this case is that over the studied range of wavelengths the lower fluid layer can be considered infinitely deep [$k(H - h) > 3$]. Comparison of Figs. 5 and 7 shows that for small values of $\bar{\delta}$ the coefficients C_x and C_y for the body beneath the pycnocline are considerably smaller than the corresponding coefficients for the body above the pycnocline. And the subsequent effect of the parameter of $\bar{\delta}$ on C_x and C_y is also very significant. The greatest wave loads take place when the elliptic cylinder is partially immersed in the pycnocline. In this case, phenomena such as emergence of the body from water are observed, and the vertical and horizontal forces increase by a factor of 1.5. A further increase in the pycnocline thickness leads to a marked decrease in the wave loads. However, in both cases of body location near the pycnocline, no complete compensation of the vertical forces was observed, although the parameter α was varied within $0.1 < \alpha < \infty$. With an increase in pycnocline thickness, the amplitude of the vertical forces decreases roughly by a factor of 2.

The change in the character of the force action of internal waves with increasing $\bar{\delta}$ can be illustrated by hodographs of the total force vector, which are shown in Fig. 8 for the cylinder located above (a) and beneath (b) the pycnocline. The shape of the curves is of greatest interest, and, therefore, the length of the force vector **R** in each experiment was normalized to the amplitude of the horizontal force F_x ($\bar{F}_{x,y} = R_{x,y}/F_x$ are plotted along the axes, and the arrows show the path direction). For small values of $\bar{\delta}$ the hodographs of the force vector are curves close to an ellipse. In Fig. 8a, $\bar{\delta} = 1.3$ and $\bar{k} = 0.6$, and in Fig. 8b, $\bar{\delta} = 0.4$ and $\bar{k} = 0.29$ (points 1 and the dashed curves). As $\bar{\delta}$ increases, a clearly distinct direction appears, along which the resulting force action is maximal. In Fig. 8a, $\bar{\delta} = 2.2$ and $\bar{k} = 0.58$, and in Fig. 8b, $\bar{\delta} = 1.6$ and $\bar{k} = 0.28$ (points 2 and solid curves). In the experiments this direction differed from the horizontal direction by an angle of up to 45°. The amplitudes of the forces acting perpendicular to this direction were smaller by a factor of 5–6. The curves in Fig. 8 correspond to values of $\bar{k}$ that differ by not more than 3.5% from one another. The experiments show that a change in the parameter $\bar{k}$ for a fixed value of $\bar{\delta}$ has a weak effect on the shape of the curves.

The character of changes in the hodographs of the vector of the total force suggests that, under the action of internal waves of the first mode on a body located in a wide pycnocline, small-scale internal waves

such as those described by the "ray" theory are generated near the body [8, 16]. In this case, a peculiar "polarization" of the force action takes place, and the interlayer with a linear density distribution and the Brunt–Väisälä frequency close to $N_{\max}$ appears to make the greatest contribution to the choice of the direction of the maximum force action. The angle θ, which characterizes the line along which the force action is maximal, is defined by $\theta = \arcsin(\omega/N_{\max})$ for the hodographs obtained in the experiments. The choice of the sign of the angle depended on the direction of orbital motion of the fluid particles in each layer. Therefore, the cases of body location above and beneath the pycnocline turned out to be mirror-symmetrical, as is evident from comparison of Fig. 8a and 8b.

It should be noted that the rotation of the total force vector, which coincides with the direction of orbital motion of the fluid particles in each layer, does not depend on $\bar{\delta}$, although in one case (Fig. 8) vertical loads are determined by inertial forces (dashed curves and points 1), and in the other case by buoyancy forces (solid lines and points 2).

The authors are grateful to I. V. Sturova for useful discussion of the results.

This work was supported by the International Science Foundation and the Russian Government (Grant JHX100).

REFERENCES

1. A. R. Osborne, T. L. Burch, and R. I. Scarlet, "The influence of internal waves on deep-water drilling," *J. Petroleum Tech.*, **30**, October, 1497–1504 (1978).
2. Yu. V. Razumeenko, "Laboratory modeling of the interaction of internal waves with underwater apparatus," in: *Problems of Stratified Flows*, Abstracts of All-Union Conf., Kanev (1991), Part. 2.
3. E. V. Ermanyuk, "Experimental study of the force interaction of internal waves on a stationary sphere," *Prikl. Mekh. Tekh. Fiz.*, **34**, No. 4, 103–107 (1993).
4. I. V. Sturova, "One-dimensional problem on the hydrodynamic rolling of a submerged body without motion in a two-layer fluid," *Izv. Ross. Akad. Nauk, Mekh. Zhidk. Gaza*, No. 3, 144–155 (1994).
5. I. V. Sturova, "One-dimensional problem on hydrodynamic rolling of a submerged body with motion in a two-layer fluid," *Prikl. Mekh. Tekh. Fiz.*, **35**, No. 5, 32–44 (1994).
6. J. Lighthill, "Fundamentals concerning loading on offshore structures," *J. Fluid Mech.*, **173**, 667–683 (1986).
7. Yu. V. Razumeenko, "Changeability of hydrophysical ocean fields, problems of maneuverability of submerged objects in real ocean," in: *Int. Symp. on Ship Hydrodynamics*, Saint Petersburg (1995), pp. 275–288.
8. O. M. Phillips, *The Dynamics of the Upper Ocean Layer*, Cambridge Univ. Press (1966).
9. I. V. Sturova, "The effect of anomalous dispersion relations on the dispersion and generation of internal waves," *Prikl. Mekh. Tekh. Fiz.*, **35**, No. 3, 47–54 (1994).
10. V. I. Bukreev, N. V. Gavrilov, and A. V. Gusev, "Internal waves in a pycnocline for a wing moving over a barrier," *Prikl. Mekh. Tekh. Fiz.*, **32**, No. 4, 68–74 (1991).
11. G. Moberg, *Wave Forces on a Vertical Slender Cylinder* (Chalmers Univ. Technol. Rep. Ser. A:16), Goteborg (1988).
12. T. Sarpkaya, "Forces on a circular cylinder in viscous oscillatory flow at low Keulegan–Carpenter numbers," *J. Fluid Mech.*, **165**, 61–77 (1986).
13. J. R. Chaplin, "Nonlinear forces on a horizontal cylinder beneath waves," *J. Fluid Mech.*, **147**, 449–464 (1984).
14. N. E. Kochin, I. A. Kibel', N. V. Rose, *Theoretical Hydromechanics* [in Russian], Fizmatgiz, Moscow (1963), Part 1.
15. M. S. Longuet-Higgins, "The mean forces exerted by waves on floating or submerged bodies with applications to sand bars and wave power machines," *Proc. R. Soc. London*, **A352**, 463–480 (1977).
16. J. S. Turner, *Buoyancy Effects in Fluids*, Cambridge Univ. Press (1973).